Timescales of carbon turnover in soils with mixed crystalline mineralogies

Lesego Khomo[1,a], Susan Trumbore[1,2], Carleton R. Bern[3], and Oliver A. Chadwick[4]

[1]Department of Biogeochemical Processes, Max Planck Institute for Biogeochemistry, Jena, Germany
[2]Department of Earth System Science, University of California, Irvine, USA
[3]Crustal Geophysics and Geochemistry Science Center, US Geological Survey, Denver, USA
[4]Department of Geography, University of California, Santa Barbara, USA
[a]now at: Department of Environmental Sciences, UNISA (University of South Africa), Johannesburg,
South Africa

Correspondence to: Susan Trumbore (trumbore@bgc-jena.mpg.de)

Abstract. Organic matter–mineral associations stabilize much of the carbon (C) stored globally in soils. Metastable short-range-order (SRO) minerals such as allophane and ferrihydrite provide one mechanism for long-term stabilization of organic matter in young soil. However, in soils with few SRO minerals and a predominance of crystalline aluminosilicate or Fe (and Al) oxyhydroxide, C turnover should be governed by chemisorption with those minerals. Here, we correlate mineral composition from soils containing small amounts of SRO minerals with mean turnover time (TT) of C estimated from radiocarbon (^{14}C) in bulk soil, free light fraction and mineral-associated organic matter. We varied the mineral amount and composition by sampling ancient soils formed on different lithologies in arid to subhumid climates in Kruger National Park (KNP), South Africa. Mineral contents in bulk soils were assessed using chemical extractions to quantify Fe oxyhydroxides and SRO minerals. Because of our interest in the role of silicate clay mineralogy, particularly smectite (2 : 1) and kaolinite (1 : 1), we separately quantified the mineralogy of the clay-sized fraction using X-ray diffraction (XRD) and measured ^{14}C on the same fraction.

Density separation demonstrated that mineral associated C accounted for 40–70 % of bulk soil organic C in A and B1 horizons for granite, nephelinite and arid-zone gabbro soils, and > 80 % in other soils. Organic matter strongly associated with the isolated clay-sized fraction represented only 9–47 % of the bulk soil C. The mean TT of C strongly associated with the clay-sized fraction increased with the amount of smectite (2 : 1 clays); in samples with > 40 % smectite it averaged 1020 ± 460 years. The C not strongly associated with clay-sized minerals, including a combination of low-density C, the C associated with minerals of sizes between 2 μm and 2 cm (including Fe oxyhydroxides as coatings), and C removed from clay-sized material by 2 % hydrogen peroxide had TTs averaging 190 ± 190 years in surface horizons. Summed over the bulk soil profile, we found that smectite content correlated with the mean TT of bulk soil C across varied lithologies. The SRO mineral content in KNP soils was generally very low, except for the soils developed on gabbros under more humid climate that also had very high Fe and C contents with a surprisingly short, mean C TTs. In younger landscapes, SRO minerals are metastable and sequester C for long timescales. We hypothesize that in the KNP, SRO minerals represent a transient stage of mineral evolution and therefore lock up C for a shorter time.

Overall, we found crystalline Fe-oxyhydroxides (determined as the difference between Fe in dithionate citrate and oxalate extractions) to be the strongest predictor for soil C content, while the mean TT of soil C was best predicted from the amount of smectite, which was also related to more easily measured bulk properties such as cation exchange capacity or pH. Combined with previous research on C turnover times in 2 : 1 vs. 1 : 1 clays, our results hold promise for predicting C inventory and persistence based on intrinsic timescales of specific carbon–mineral interactions.

1 Introduction

The radiocarbon content of soil C provides a measure of how long C can persist in soils (Trumbore, 2009). A working hypothesis is that the relative strengths of mineral–carbon interactions will be reflected in the radiocarbon content of the associated organic C. For example, 1 : 1 silicate clays with inherently low surface area, such as kaolinite, have limited sorptive capacity and retain C over relatively short timescales (Heckman et al., 2009; Sollins et al., 2009). In contrast, 2 : 1 clays with high charge density and high surface area, such as smectite, have higher affinity for C and thus retain it for relatively longer. In soils where the predominant minerals are smectites, organic C has older radiocarbon ages than in soils dominated by kaolinite (Wattel-Koekkoek et al., 2003; Poch et al., 2015). Soils in which much of the C is associated with high surface area short-range-order (SRO) minerals like Fe and Al oxyhydroxides contain organic C that has persisted for many millennia (Torn et al., 1997).

In soils of mixed mineralogy, several organic-mineral interaction mechanisms operate simultaneously, requiring multiple timescales for organic carbon persistence to explain radiocarbon measurements (e.g., Schrumpf and Kaiser, 2015; Schrumpf et al., 2013; Wattel-Koekkoek and Buurman, 2004).

The ability to quantitatively link specific mineral stabilization mechanisms with radiocarbon-based timescales of turnover is hampered because the operationally defined procedures used to quantify soil mineral content mostly differ from those used to separate organic C into fractions that differ in radiocarbon content. Two main approaches have been used to address this issue. One approach is to select samples for analysis from distinctly different global environments and use samples dominated by single mineral compositions (e.g., as described above; Wattel-Koekkoek et al., 2003). Another approach is to sample soils along environmental gradients, and to correlate C age with the abundance of specific mineral stabilization mechanisms (e.g., Torn et al., 1997; Masiello et al., 2004; Lawrence et al., 2015), but often without full quantification of all the possible controls on C storage. Relatively few studies combine measures of the amounts and age of C in soil with quantitative measures of mineralogy. In particular, more studies are needed that focus on the C stabilization behavior of mature soils where long-term depletion of primary minerals and ripening of secondary minerals provides an environment dominated by well crystallized compounds that have relatively low chemical reactivity (see Wattel-Koekoek et al., 2003; Torn et al., 1997). In regions with long-term tectonic and climatic stability, such as parts of the tropics and subtropics (Paton et al., 1995), it is possible that the differences in C sorption between 2 : 1 and 1 : 1 clays could be one of the most important controls on C storage and turnover.

Here, we analyze a lithosequence of arid to subhumid savanna soils developed on the Kaapvaal Craton and associated post-Gondwana breakup lavas in Kruger National Park (KNP) South Africa (SA). Low rates of landscape erosion and exceptionally long soil residence times (Chadwick et al., 2013) ensure that nearly all soil minerals have evolved past the metastable SRO stage and that there are few free trivalent metal ions available for direct sorption by organic ligands (Khomo et al., 2011, 2012). We evaluate radiocarbon (^{14}C) in bulk soil, and fractions separated by density into free particulate and mineral-associated components. In parallel, we used chemical extractions of bulk soils to quantify Fe oxyhydroxides and SRO minerals, and quantified allied properties such as cation exchange capacity. Because of our interest in the role of silicate clay mineralogy, particularly smectite (2 : 1) and kaolinite (1 : 1), we separated the clay-sized fraction for X-ray diffraction (XRD) analysis of mineralogy, and measured ^{14}C on the same fraction.

Our specific research questions reflect the inherent limitations in combining different methods to quantify minerals and organic matter as follows. (1) How do the amount and radiocarbon content of bulk, low density ($< 1.7\,\mathrm{g\,cm^{-3}}$), and dense ($> 1.7\,\mathrm{g\,cm^{-3}}$) fractions vary among soils developed on different parent materials present in the Kruger National Park? (2) Can we define relationships between minerals and the amount and mean turnover time (TT) (derived from ^{14}C) of carbon? (3) Can such relationships be extrapolated from specific soil samples to entire soil profiles and across soils with contrasting mineralogy? Our overall goal is to find relationships that allow us to predict the amount and TT of carbon across broader landscapes with similar soil forming factors.

2 Materials and methods

2.1 Field sites

To evaluate mineralogical controls on C storage and turnover we sampled soils across gradients in geology, climate, and topography in KNP. Soil residence times, estimated from average regolith depth and erosion rates determined using cosmogenic isotopes are $> 10^5$ years (Chadwick et al., 2013), providing ample time for crystalline mineral differentiation, ripening, and depletion of metastable SRO minerals. In addition to strong geological differences across KNP, variation in clay mineralogy is imposed by a regional north–south gradient in rainfall that ranges from about 470 to 740 mm annually, and locally by differentiation of clay content along hillslopes. Under this setting, we can focus on organic matter–mineral interactions associated with differences in silicate clays and secondary Fe and Al oxyhydroxides in an environmental regime expected to have few SRO minerals.

We sampled soils underlain by five geological units: rhyolite, granite, an olivine-rich picrite basalt (black basalt), an
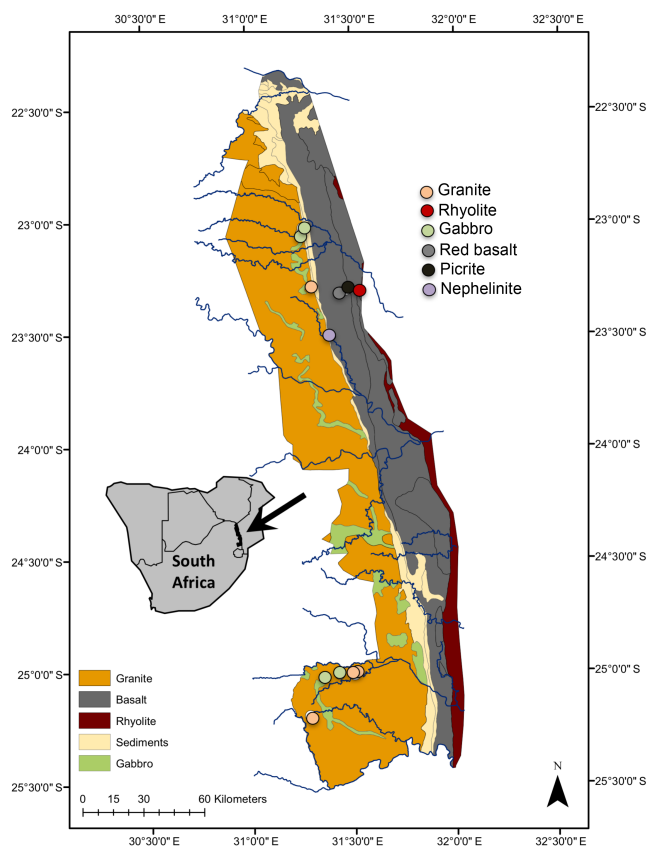
Figure 1. Locations and lithology of parent materials where soils were sampled for this study. Rainfall decreases from $\sim 740\ \mathrm{mm\ a^{-1}}$ in the southern end of the park to $\sim 450\ \mathrm{mm\ a^{-1}}$ in the northern end of the park.

olivine-poor basalt (red basalt), and nephelinite (Venter et al., 2003) (Table 1, Fig. 1). Each of the lithologies were sampled in the northern arid zone, with mean annual temperature of $23\ ^{\circ}\mathrm{C}$ and $\sim 470\ \mathrm{mm}$ annual precipitation. We also sampled soils developed on granite, gabbro, and mixed granite/gabbro parent materials in the south of the park where rainfall ranges from ~ 550 to $740\ \mathrm{mm}$ per year (Table 1). Samples were collected along watershed divides, i.e., hill crests in the gently rolling landscape, although we include data for soils collected along one toposequence at $550\ \mathrm{mm}$ of rain to broaden the range of minerals formed on granitic soils (Khomo et al., 2011, 2012; Bern et al., 2011).

2.2 Bulk soil characterization

Soil profiles were sampled by horizon to bedrock where possible and described and classified using standard techniques. Soil depth ranged from $30\ \mathrm{cm}$ to about $2\ \mathrm{m}$. Following air-drying, the samples were sieved to $< 2\ \mathrm{mm}$ to remove rocks and roots. Air-dried samples were homogenized and subsampled for physical, chemical, isotopic, and mineralogical analyses. Bulk density was measured as the mass of oven-dry soil

in a core of known volume. The amount of clay-sized material ($< 2\ \mu\mathrm{m}$ size fraction) was determined by the hydrometer method (Soil Survey Staff, 2014). The concentration of exchangeable base cations was determined by atomic absorption spectroscopy after extraction with $1\ \mathrm{M}$ ammonium acetate buffered at pH 7. Cation exchange capacity (CEC) was determined by extracting the ammonium saturated samples with a $1\ \mathrm{M}$ potassium chloride solution and determining ammonium by Lachat autoanalyzer. We report CEC corrected for the contribution of organic matter by assuming a contribution of $200\ \mathrm{cmol}(+)$ per kilogram of organic C (as measured using an elemental analyzer; Soil Survey Staff, 2014).

SRO minerals (aluminosilicate or Fe oxyhydroxides that are minimally polymerized) were extracted from bulk soils using acid ammonium oxalate in the dark (Schwertmann, 1973). Iron (Fe(o)) and Al (Al(o)) from the extract were measured by inductively coupled plasma-optical emission spectrometry. We also applied a standard dithionite citrate bicarbonate (DCB) extraction and report the Fe concentration in this solution as Fe(d) (Mehra and Jackson, 1960). Total crystalline Fe oxyhydroxides are defined as Fe(d)–Fe(o). Carbon and nitrogen (N) content were determined by combustion on a vario MAX cube CN elemental analyzer. To determine if soils contained pedogenic soil carbonates, inorganic C was determined on the residue after dry combustion of bulk samples at $450\ ^{\circ}\mathrm{C}$ for $16\ \mathrm{h}$ (Steinbeiss et al., 2008) and organic C was calculated as the difference between total C and inorganic C. Carbonates were present in the red basalt and two of the arid-zone gabbro profiles; carbonates in upper horizons were mostly present as individual particles (i.e., not coatings) presumably derived from more massive carbonates in a Bk horizon below.

2.3 Clay-sized material for XRD analysis

To isolate and prepare clay-sized material for XRD measurement of mineralogy, we started with bulk soil material. Sand-sized material was removed first by wet-sieving and then the clay-sized ($< 2\ \mu\mathrm{m}$) fraction for XRD was extracted following dispersion with $5\ \%$ sodium hexametaphosphate and $2\ \%$ H_2O_2 with three rounds of sedimentation and decantation in a $1\ \mathrm{L}$ cylinder (Soil Survey Staff, 2014). The decanted material containing clay-sized material was evaporated and freeze-dried. The $2\ \%$ H_2O_2 treatment, a standard pretreatment for isolation of clay-sized material for XRD measurement, also removed organic C and we waited for bubble formation (presumably from oxidation of organic matter) to cease before the first decanting procedure. Organic matter oxidized by this treatment included free particulate organic C, such as small plant fragments, that would also float in a solution of $1.7\ \mathrm{g\ cm^{-3}}$ (i.e., our low-density fraction in 2.4 below). However, this treatment can also remove organic C that is weakly associated to clay-sized mineral surfaces. Thus, we refer to material isolated this way as the "clay-sized XRD fraction" and assume that any C still in that fraction must be

Table 1. Profile names used in the text, parent material lithology, mean annual precipitation (MAP), year of collection, locations, and classification of the soil profiles used for this study.

Profile name	Lithology	MAP (mm)	Slope position	Year	Latitude (easting)	Longitude (northing)	Classification
GR-450-C	Granite	450	Crest	2004	322 713	7 452 153	Haplocambid
GA-450-C	Gabbro	450	Crest	2010	321 956	7 449 291	Calciustoll
RH-450-C	Rhyolite	450	Crest	2010	351 375	7 421 676	Haplocambid
NE-450-C	Nephelinite	450	Crest	2010	336 567	7 398 988	Ustorthent
BB-450-C	Black basalt	450	Crest	2009	341 888	7 420 588	Haplustert
RB-450-C	Red basalt	450	Crest	2009	344 120	7 421 754	Duritorrand
GR-550-C	Granite	550	Crest	2006	348 678	7 231 971	Ustorthent
GR-550-S	Granite	550	Seepline	2006	348 755	7 231 990	Dystrustept
GR-550-T	Granite	550	Footslope	2006	348 831	7 231 986	Natrusalf
MG-550-C	Mixed granite	550	Crest	2010	341 298	7 232 342	Ustorthent
MG-550-C2	Mixed granite	550	Crest	2010	341 298	7 232 342	Ustorthent
GA-550-C	Gabbro	550	Crest	2005	333 525	7 230 774	–
GA-740-C1	Gabbro	740	Crest	2010	329 124	7 218 015	Haplotorrert
GA-740-C2	Gabbro	740	Crest	2010	329 124	7 218 015	Haplotorrert
GR-740-C	Granite	740	Crest	2004	326 823	7 211 630	Dystrustept

strongly associated with mineral surfaces. We estimate the C and C isotope content of C removed during isolation of the clay-sized XRD fraction using mass balance.

Splits of the clay-sized material were subjected to standard clay mineral identification routines including saturation with KCl and MgCl₂ before qualitative and quantitative analysis by XRD. For mineral identification, peel-mounts of oriented clay-sized material were made by transferring the sample onto microprobe glass slides from 0.42 μm cellulose nitrate membrane filters where they had been oriented by vacuum (Pollastro, 1982). For mineral quantification, the clay-size fraction was micronized in methanol with 10 % corundum by sample weight, dried, passed through a 50 μm sieve, and placed into side-packed powder mounts (Eberl, 2003). XRD spectra were generated with a Siemens D500 diffractometer using Cu Kα radiation fitted with a graphite monochrometer configured to 35 mA and 40 kV. Mineral quantification was done using the RockJock software (Eberl, 2003) and results were summed by mineral group. Quantitative mineral data for the clay-sized XRD fraction from the granitic toposequence at 550 mm rainfall have been previously published (Khomo et al., 2011). All mineralogy data are normalized to sum to 100 %.

2.4　Density separation

For depth intervals identified as A horizons, where fresh plant inputs are largest, we performed a density separation on a subsample of soil. We used a heavy sodium polytungstate liquid (1.7 g cm⁻³) to separate the sample into free light fraction (fLF) and heavy fraction (HF) (Schrumpf et al., 2013, modified to a density of 1.7 g cm⁻³). A density of 1.7 g cm⁻³ is sufficient to separate minerals from fresh particulate organic material especially in soils with minimal SRO miner-

als that can have low densities (Castanha et al., 2008). Between 10 and 15 g of soil was added to 100 mL sodium poly-tungstate solution and gently shaken on a horizontal shaker for 10 min, ultrasonicated at 60 J mL⁻¹ for 2.5 min, then centrifuged at 3500 rpm for 30 min. Because of the low energy used, we consider this fraction to be the fLF, i.e., there may still be some additional particulate material of low density trapped in aggregates that are not dispersed. The floating fLF was concentrated on filter paper (1.6 μm glass microfiber discs) using a light vacuum. The sinking material was resuspended in the heavy solution and the steps repeated without the ultrasonic disaggregation until no more floating fLF was observed (usually three times). The fLF was rinsed with a liter of water to remove the heavy liquid, then freeze-dried. Visible, very fine roots were removed by hand (Castanha et al., 2008); coarser roots were removed by previously sieving. However, the efficiency of these procedures varies so we used the density separation to ensure all fine roots were removed from the sample. The remaining root-free fLF was ground to homogenize it for C isotope measurements. Somewhat lower C contents in the root-free fLF fraction in this paper compared to other published studies that used different procedures are likely due to removal of roots, combined with small amounts of mineral inclusion that were unavoidable as small-sized material was difficult to separate using the centrifuge (no flocculants were added).

We estimated the overall mass balance of the procedure by combining the mass and C contents of the different fractions (roots, root-free fLF, and HF) with the mass and C content of the original bulk sample (Supplement Table S1); in A horizons we lost 2–15 % of the original C (Table S2), likely through dissolution in the dense liquid (Castanha et al., 2008)

Table 2. Mineralogy determined on clay-sized XRD fraction for selected soils (mostly mafic soils that had higher clay contents). Abbreviations are Hor, soil horizon, Q: quartz, F: feldspars, Cal: calcite, O: oxides, K: kaolins, S: smectites, Ch: chlorites, and M: micas. Complete data can be found in Table S1.

Identifier	Hor	Clay	Q	F	Cal	O	K	S	Ch	M
		(%)	Percentage of clay-sized fraction							
NE-450-C	A	30	1	1	0	15	24	47	0	12
NE-450-C	Bw1	40	1	1	0	14	26	48	0	9
BB-450-C	A1	39	1	0	0	0	6	92	0	0
BB-450-C	Bw1	43	2	0	0	0	5	93	0	0
RB-450-C	A1	36	1	0	0	0	0	99	0	0
RB-450-C	Bk2	46	2	0	0	0	0	98	0	0
GA-450-C	A	15	2	2	0	7	0	67	0	22
GA-450-C	Bw1	25	1	9	6	10	0	43	3	28
GA-740-C1	A	20	0	1	0	14	10	60	6	9
GA-740-C2	Bw1	25	0	1	0	8	16	68	6	1
GA-740-C3	Bw2	10	0	0	0	14	3	77	3	3
GR-550-C*	A	14	0	0	0	0	79	0	21	0
GR-550-C*	Bw2	17	0	0	0	0	79	1	21	0
GR-550-S*	A	6	0	0	0	0	76	17	7	0
GR-550-S*	Bw2	7	0	0	0	0	65	25	11	0
GR-550-T*	A	25	0	0	0	0	57	26	17	0
GR-550-T*	2Btn2	47	0	0	0	0	53	23	15	10

* Data are from Khomo et al. (2011).

Thus, our analyses of C and radiocarbon in fractions contain overlapping information. For example, we can assume that all of the C and ^{14}C strongly associated to the clay-sized XRD fraction (Clay$_{XRD}$) is also found in the HF. The C removed during isolation of Clay$_{XRD}$ contains a mixture of C associated with minerals larger than clay-sized (e.g., a component of HF) as well as root and root-free fLF C (see also Results, Fig. 4). While it would have been preferable to do a sequential extraction, the separation of sufficient clay-sized material for mineralogy and C isotope analyses from the HF fraction would have been costly and required large amounts of material (particularly for sandy soils with low clay content).

Similarly, our mineralogical information has some overlapping components. For example, in the Clay$_{XRD}$, we report Fe oxyhydroxides as the sum of minerals such as goethite, magnetite, maghemite, and ilmenite (Table S1). We do not normally refer to this fraction, but rather to the bulk soil measurement of Fe oxyhydroxides, which we define as the Fe compounds that are dissolved by a standard dithionite citrate extraction but not by the standard oxalate extraction (i.e., Fe(d)–Fe(o)). These compounds are assumed to be pedogenic Fe (though some amount of geogenic Fe is possibly also dissolved), and includes the Clay$_{XRD}$ Fe oxyhydroxides as well as coatings on minerals with sizes $> 2\,\mu m$ but $< 2\,mm$.

2.5 Carbon isotopes

Radiocarbon (^{14}C) was determined by accelerator mass spectrometry (AMS). For determination of ^{14}C in organic samples, an amount of material (bulk soil, HF, fLF, or clay)

needed to yield $\sim 1\,mg\,C$ was weighed into a precombusted quartz tube with CuO wire. The tube was evacuated, sealed with a torch, and placed in a $900\,°C$ furnace for 3 h. The resulting CO_2 was purified on a vacuum line, and an aliquot was removed for determination of $^{13}CO_2$ using a gas bench coupled to an isotope ratio mass spectrometer (Xu et al., 2007). The remaining CO_2 was reduced to graphite using a sealed tube zinc reduction method (Xu et al., 2007), and isotopic compositions were measured at the W.M. Keck Carbon Cycle AMS facility at the University of California, Irvine. Samples containing inorganic C were acidified with 1N HCl until the solution pH was below 6, and then dried and analyzed as above. Carbonates were normally present as distinct sand-sized or larger grains, and were present only in the black basalt and the dry gabbro samples; we also used the ^{13}C signature of the combusted sample to indicate that carbonate did not contribute significantly to the measured sample C. For the black basal soil, we analyzed ^{14}C in pedogenic carbonates by collecting and purifying the CO_2 evolved during acidification, then reducing it to graphite as for organic C samples.

Radiocarbon data are reported as Δ^{14}C, the deviation from unity, in parts per thousand, between the ratio of ^{14}C / ^{12}C in the sample divided by that of preindustrial wood (the standard). The potential influence of mass-dependent fractionation of isotopes is accounted for by reporting the ^{14}C / ^{12}C ratio corrected to a common δ^{13}C value ($-25\,‰$), and assuming that ^{14}C is fractionated twice as much as ^{13}C by mass-dependent processes (Stuiver and Polach, 1977). Therefore, differences in Δ^{14}C between samples reflect time or mixing rather than isotope fractionation. In these units, $\Delta^{14}C = 0\,‰$ is equivalent to the standard. Values $> 0\,‰$ indicate the presence of ^{14}C produced by atmospheric thermonuclear weapons testing in the early 1960s. Values $< 0\,‰$ indicate that radiocarbon has had time to radioactively decay (half-life $= 5730$ years). Long-term accuracy for samples measured at the W.M. Keck CCAMS facility is $\pm 3\,‰$ for radiocarbon expressed as Δ^{14}C and $\pm 0.1\,‰$ for δ^{13}C.

We also used the radiocarbon data to estimate the mean TT of soil C in the profile using a one-pool model that includes incorporation of bomb ^{14}C in the last few decades and assumes steady state (see Torn et al., 1997; Trumbore, 2009). Specifically, we used the SoilR package (Sierra et al., 2014) to calculate the predicted radiocarbon signature for such a one-pool, steady-state model in the year of sampling (R code is included in the Supplement). For cases where two turnover times yielded the same Δ^{14}C in the year of sampling (i.e., in cases where Δ^{14}C is $> 0\,‰$), we report both TTs for the root-free fLF, but only the longer turnover time as it is more consistent with the fluxes of C into and out of the mineral associated and bulk fractions (see Gaudinski et al., 2000). The one-pool model is clearly an oversimplification, but is useful for translating radiocarbon data into average timescales of stabilization. The use of a mean TT also provides a way to compare data from samples collected in different years

(2004–2011; Table 1). We want to emphasize that these TTs only have meaning in the context of the assumptions used to generate them – they refer to C in a single, homogeneous pool at steady state.

We report C concentration and isotope data for individual horizons as well as whole-profile averages (e.g., as in Masiello et al., 2004). Mean C isotope ratios and mean estimated turnover times for whole profiles were calculated as averages, the carbon mass weighted by horizon and calculated from measured bulk soil ^{13}C and ^{14}C values.

2.6 Statistics

Graphs, including regression analyses, were produced with R (R Core Team, 2015). Correlation matrices were produced using the R package Hmisc (Harrell Jr. et al., 2016). The TTs were calculated with the SoilR package (Sierra et al., 2014).

3 Results

3.1 Mineralogy

With few exceptions, these ancient soils contained low amounts (< 0.3 wt. %) of oxalate extractable Fe and Al presumed to be derived from SRO minerals (complete data are given in Table S1). Only nephelinite-derived (0.5–0.9 wt. %) and subhumid gabbro soils had greater (2.9 wt. %) concentrations of oxalate extractable Al + Fe. Crystalline Fe oxyhydroxides determined as Fe(d)–Fe(o) ranged from 0 % in a periodically anoxic "seep" zone in the granitic toposequence to 5.2 wt. % in the nephelinite soil.

The clay-sized XRD fraction made up ≤ 15 % of the < 2 mm mass for soils developed at crest positions on granites and rhyolites, but up to 35–50 % in the red and black basalt, arid-zone gabbro and nephelinite soils, and at the toeslope of the granitic toposequence (Tables 2, S1). With a few exceptions, the amount of clay-sized material increased with soil depth.

Within the clay-size XRD fraction, the sum of smectite, kaolinite, micas and chlorite and crystalline Fe minerals generally made up over 90 % of the quantified mineralogy (Table 2). Smectite was present in all of the isolated clays except the granite crest under relatively high (740 mm) rainfall and dominated the clay fraction in red (> 90 %) and black basalts (> 99 %; Table 2). Kaolinite was common in most soils but rare in the arid-zone gabbro and the two basalts. Crystalline Fe oxide minerals identified by X-ray diffraction made up 3–26 % of the clay-sized fraction for most soils but < 1 % in the smectite-dominated red and black basalts (Table 2).

Comparison of Fe oxyhydroxide abundance estimated by scaling quantitative XRD in the clay fraction to the whole soil (i.e., multiplying the weight percent clay times the Fe oxide content measured by XRD) with that measured by extraction with DCB and oxalate in the bulk soil showed overall correspondence (see Fig. S1) but with much scatter.
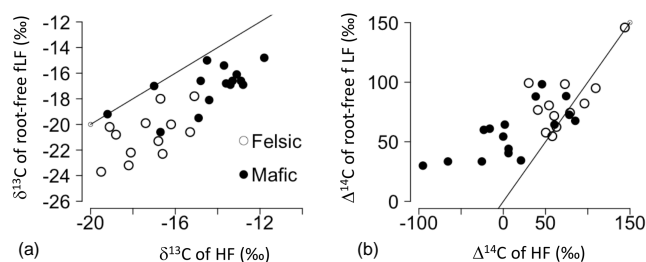

Figure 2. Comparison of ^{13}C (**a**) and ^{14}C (**b**) in root-free free light fraction (root-free fLF) and heavy fraction (HF) organic C for individual samples from A horizons (see Table 3). Felsic lithologies (white circles) include soils developed on granite and rhyolite; mafic lithologies (black circles) include soils developed on gabbros, basalts, and nephelinite. The 1 : 1 correlation line is plotted for reference.

3.2 C in density fractions of A and B1 horizons

The root-free fLF isolated from A horizons had C concentrations of 1.0–3.7 gC kg^{-1} (Table 3), with lower concentrations in the soils derived from rhyolite and the two basalts (1.0–1.6 % gC kg^{-1}). As mentioned above, removal of roots and the inclusion of some clay-sized material during filtration can result in lower values than expected if the root-free fLF is only fresh plant material. In general, carbon in the root-free fLF made up only 10–20 % of bulk C, even in surface soils (Table S1). Mineral-associated HF had lower C concentrations but comprised more of the bulk soil mass and represented 40–70 % of bulk soil C for granites, nephelinite and dry gabbro soils, and > 80 % in other soils (Table 3).

Root-free fLF δ^{13}C ranged from −24 to −14.5‰ (Table 3), reflecting a mixture of C3 and C4 vegetation sources. We found no relationship between root-free fLF δ^{13}C or HF δ^{13}C with rainfall, but mafic soils were consistently more enriched in δ^{13}C in both fractions compared to felsic soils (Fig. 2a). Radiocarbon signatures of root-free fLF (that includes char as well as plant fragments) varied from values close to those measured in annual grasses in 2010 (+35‰ in Δ^{14}C) up to +145‰ (Fig. 2b). For surface horizons, the one-pool model yielded two possible turnover times for most of the root-free fLF Δ^{14}C. Assuming the shorter of the two for soil A horizons (normally 0–2 cm), yielded TTs from < 1 to 8 years, while assuming the longer TT yielded 45–185 years (Table 3). For the black basalt and arid-zone gabbro soil A horizons, only longer root-free fLF TTs (125–185 years) were consistent with observed Δ^{14}C signatures. The TT of both root-free fLF and HF increased with depth. Fine roots picked from root-free fLF in the red basalt soil had radiocarbon signatures equivalent to TT < 1 year regardless of depth (Table S1) and δ^{13}C signatures of −12 to −16‰.

The δ^{13}C of HF averaged ~ 3–4‰ more enriched than δ^{13}C of root-free fLF from the same soil (Fig. 2a). Radiocarbon signatures in mafic soil HF were generally much more depleted in ^{14}C than root-free fLF from the same horizon

Table 3. Carbon and carbon isotope signatures of heavy ($> 1.7\,\mathrm{g\,cc^{-1}}$) and root-free free light fraction carbon. Turnover times (TTs) were estimated using the steady state, one-pool model described in the text. When two TTs were possible, we show both options for the root-free fLF but only the longer one for the heavy fraction.

Identifier	Depth (cm)	Total C in HF	Root-free free light fraction C_{org} ($\mathrm{gC\,kg^{-1}}$)	$\delta^{13}C‰$	$\Delta^{14}C‰$	TT (year)	Heavy fraction C_{org} ($\mathrm{gC\,kg^{-1}}$)	$\delta^{13}C‰$	$\Delta^{14}C‰$	TT (year)
GR-450-C	0–23	0.59	3.70	−23.7	99.3	5, 75	0.05	−19.5	30.1	195
	23–45	1.06*	2.46	−18.9	125.6	8, 50	0.04	−17.5	−35.9	510
GA-450-C1	0–2	na	3.42	−16.8	44.1	155	na	−13.6	6.2	275
	2–12	na	4.23	−15.0	34.4	180	na	−14.5	20.9	225
RH-450-C	0–3	0.81	1.66	−23.2	98.4	8, 75	0.07	−18.2	72.9	55
	3–15	0.83	0.19	−20.0	76.7	5, 100	0.05	−16.2	40.9	165
NE-450-C	0–2	0.65	3.13	−20.6	88.3	8, 85	0.42	−16.7	74.4	105
	2-18	0.76	3.08	−19.5	64.4	4, 120	0.24	−14.9	1.8	300
RB-450-C	0–4	0.82	1.16	−16.6	60.0	3, 125	0.18	−14.8	−23.1	425
	4–15	0.69	1.00	−16.6	30.0	195	0.14	−13.3	−95.2	985
	15–30	0.92	1.00	na	na	na	0.14	−13.3	−152	1560
	30–49	0.84	1.12	na	−53.0	330	0.13	−13.3	−216	2300
BB-450-C	0–3	n.d	1.00	−15.4	33.5	185	0.15	−13.7	−25.4	440
	3–11	0.78	0.05	−16.6	33.5	185	0.16	−12.9	−65.6	735
GR-550-C	0–15	0.70	1.60	−22.2	57.7	1, 130	0.05	−18.1	50.3	145
	15–41	na	1.45	−21.9	82.3	2, 95	0.04	−17.1	59.0	130
GR-550-S	0–2	0.72	2.25	−20.8	62.4	1, 120	0.05	−18.8	62.9	120
	2–10	1.1*	2.13	−20.2	82.1	4, 95	0.04	−19.1	96.1	80
GR-550-T	0–8	0.91	2.12	−18.0	54.7	1, 135	0.08	−16.7	58.0	130
	8–15	0.69	1.52	−19.9	74.4	105	0.05	−17.4	79.0	100
MG-550- C	0–3	0.84	3.69	−22.3	71.7	5, 125	0.09	−16.6	60.2	125
	3–10	0.92	1.55	−20.6	80.5	6, 110	0.07	−15.3	54.1	135
GA-550-C	0–9	na	2.99	−28.2	98.3	5, 85	0.28	−14.4	45.8	140
	9–24	na	1.52	−13.2	88	4, 100	0.23	na	38.4	175
GA-740-C1	0–3	0.70	3.47	−16.9	72.6	1, 100	0.16	−13.4	78.2	100
	3–9	0.73	2.32	−14.8	40.5	165	0.15	−11.8	6.1	275
GA-740-C2	0–4	0.85	3.57	−16.1	67.6	4, 135	0.15	−13.1	85.2	90
	4–24	0.76	3.53	−16.9	64.4	4, 140	0.18	−12.8	60.6	125
GR-740-C	0–8	0.41	3.27	−21.3	145.8	10, 45	0.10	−16.8	143.9	45
	8–17	0.66	1.86	−17.8	95.0	4, 80	0.03	−15.1	109.4	70

* Values > 1 indicate the magnitude of errors associated with density separations; na means not analyzed.

(Fig. 2b). Felsic soils tended to have higher ^{14}C values in HF than mafic soils, though this was less true for root-free fLF fractions.

3.3 Changes in C, ^{13}C and ^{14}C with depth

Soil depths increased with increasing annual rainfall. In all soils, C and ^{14}C concentration decreased with depth. However, differences in lithology and hence mineralogy were more important controls on C and C isotopes than differences in rainfall (Fig. 3 and Table S2). Notably, soils developed on nephelinite had the highest C concentrations while felsic soils had the lowest (Fig. 3). Patterns in δ^{13}C by depth followed two general patterns. Felsic, gabbro, and nephelinite soils had large (2–6‰) increases in between the surface and ~ 10–30 cm depth then became depleted below (Fig. 3).

Red and black basalt soils experienced a $\sim 2‰$ enrichment in δ^{13}C to ~ 10 cm depth and then stayed constant. Radiocarbon declined with depth in all soils but in wetter sites (> 550 mm annual rainfall) shifted towards higher ^{14}C values at the very bottom of the profile (BC or C horizons; Table S1). The ^{14}C signatures of organic C in the red and black basalt soils were lower ($< 0‰$ at all depths, even at the surface) compared to the other soils and were the most enriched in δ^{13}C at all depths (Fig. 3).

The B horizons of the red basalt and the two arid-zone gabbro soils contained pedogenic carbonates at concentrations of up to several percent with radiocarbon ages ranging from ~ 4500–25 000 ^{14}C years, substantially lower in ^{14}C compared to organic C at the same depths (see Table S1). The carbonates in B1 horizons were generally found as distinct small but visible fragments (with ^{14}C ages up to ~ 4500 years)

Table 4. Measurements of C and isotopes in the bulk soil and clay-sized XRD fraction, the same fraction analyzed for quantitative mineralogy (Table 2). The fraction of bulk C in the clay-sized XRD fraction ($F_{clayXRD}$) and the characteristics of the C making up the rest of the bulk C are calculated using Eqs. (1)–(3) given in the text. Horizon bottom depths (Bot. depth) > 10 cm indicate B1 horizons; we excluded data from sampled depths > 20 cm. We cannot rule out the potential for carbonates making up a small fraction of the Clay$_{XRD}$ fraction for the dry gabbro (GA-450-C1) Bw horizon sample as these were not acidified prior to combustion and carbonates were found using XRD in this soil. All other Clay$_{XRD}$ samples did not contain measurable carbonates (Table 2).

| | Bot. depth | Clay-sized (< 2–μm) XRD fraction | | | | Bulk soil | | | | | Remaining C ("non-clay") | | | |
Identifier	(cm)	C_{org} (gC kg^{-1})	$\delta^{13}C$ ‰	$\Delta^{14}C$ ‰	TT (year)	C_{org} (gC kg^{-1})	$\delta^{13}C$ ‰	$\Delta^{14}C$ ‰	TT (year)	$F_{clayXRD}$	C_{org} (%)	$\delta^{13}C$ ‰	$\Delta^{14}C$ ‰	TT (year)
NE-450-C	2	0.252	−16.9	−1.5	310	0.604	−17.8	65.0	110	0.13	6.5	−17.9	69	110
NE-450-C	18	0.114	−16.8	−129.5	1330	0.304	−15.4	8.0	270	0.15	3.4	−15.3	16	240
GA-450-C1	2	0.469	−14.8	−64.6	730	0.328	−14.9	20.1	225	0.22	2.9	−14.9	58	130
GA-450-C1	12	0.235	−13.9	−145.0	1485	0.190	−13.9	−28.8	465	0.31	1.7	−13.9	43	160
RB-450-C	4	0.250	−14.1	−125.3	1275	0.194	−14.9	−16.0	385	0.47	1.5	−16.0	149	30
BB-450-C	3	0.248	−14.3	−91.7	955	0.241	−13.7	−25.4	440	0.40	2.4	−13.4	22	220
GA-450-C2	2	0.129	−16.3	−4.4	320	0.162	−16.6	22.0	220	0.12	1.7	−16.6	25	210
GA-740-C1	4	0.096	−17.6	−91.7	955	0.218	−11.8	−62.1	690	0.09	2.3	−11.6	−61	690
GA-740-C2	9	0.117	−19.1	−160.0	1650	0.176	−13.6	88.1	85	0.14	1.9	−12.9	122	55
GA-740-C2	24	0.110	−17.7	−116.1	1180	0.224	−13.4	70.0	110	0.10	2.4	−13.0	83	90

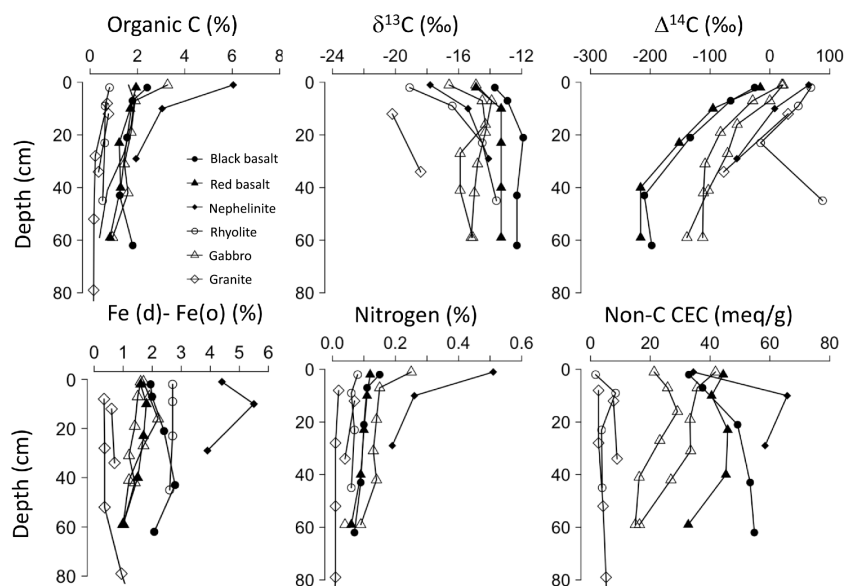**Figure 3.** Depth profiles of bulk C (top-left), $\delta^{13}C$ (top-middle), and $\Delta^{14}C$ (top-right) measured in bulk C for soil profiles developed on selected lithologies. Also shown in the lower panels are other soil bulk properties, total Fe oxyhydroxides (Fe(d)–Fe(o)) (bottom-left), total nitrogen (bottom middle), and cation exchange capacity (CEC) corrected for organic matter contributions (bottom right; see text).

and likely derived from fragmentation and upward mixing of older and more massive carbonates observed deeper in the soil. Carbonates do not influence radiocarbon or signatures reported for organic matter in these soils as they were removed prior to combustion; the efficiency of removal can be observed in the similarity between isotope signatures of organic C in red basalts (containing carbonate) and black basalts (that did not have carbonate).

3.4 Carbon inventory and C strongly associated with clay-sized XRD fraction

The concentration of C strongly associated with the Clay$_{XRD}$ fraction ranged between 0.10–0.47 gC kg^{-1} across all soils. Both the amount of C and its TT (ranging from 310 to 1330 years) increased with the amount of smectite measured in the same fraction (Table 4; Fig. 5a). For Clay$_{XRD}$ samples where smectite made up > 95 % of the total mineral content, the mean TTs were in the range of 970–1250 years. Carbon strongly associated with Clay$_{XRD}$ samples where only ~ 45 % of the mineral was smectites had the lowest TTs

(340 years). We were unable to measure radiocarbon in samples from granites due to the very low yield of clay-sized material in these soils.

Assuming bulk C has two components, a portion strongly associated with clay (Clay$_{XRD}$) and the rest of the soil C ("non-clay"), i.e., C that was removed with $> 2\,\mu m$ material (including coatings and organic matter associated with larger grains) or by the 2 % H$_2$O$_2$ treatment (including much of the LF but also organic C weakly associated with clay-sized material). We estimated the amount and radiocarbon signature of this "non-clay" component using mass balance as follows:

$$\%C_{\text{non-clay}} = (\%C_{\text{bulk}} - F_{\text{ClayXRD}} \times \%C_{\text{ClayXRD}})/ \\ (1 - F_{\text{ClayXRD}}) \qquad (1)$$

$$\Delta^{14}C_{\text{non-clay}} = \Delta^{14}C_{\text{bulk}} - F_{\text{ClayXRD}} \times \Delta^{14}C_{\text{ClayXRD}})/ \\ (1 - F_{\text{ClayXRD}}), \qquad (2)$$

where F_{ClayXRD} is the fraction of bulk C that is found in the clay-sized XRD fraction:

$$F_{\text{clayXRD}} = (\%C_{\text{clayXRD}} \times \%\text{Clay})/(\%C_{\text{bulk}} \times 100\,\%). \qquad (3)$$

For the basalts, C in the Clay$_{XRD}$ fraction made up 40–47 % of C$_{\text{bulk}}$ in the top 2 cm, increasing to 80–86 % in B horizons (see Table S1). For all other soils, the amount of C strongly associated with Clay$_{XRD}$ accounted for < 30 % of bulk C. Other than the basalt-derived soils (and deeper B horizons in the gabbros; Table S1), most bulk C was thus removed by the fractionation processes (size and H$_2$O$_2$ treatment). As estimated from mass balance, the C removed ($\Delta^{14}C_{\text{non-clay-sized}}$) in the top 18 cm was (with one exception) dominated by C fixed in the last 50 years (Table 4). The estimated TT for non-clay$_{XRD}$ C ranged from 30 to 690 years, averaging 190 ± 190 years; Table 4. The C strongly associated with Clay$_{XRD}$ (a fraction that includes not only clay minerals but up to 26 % Fe oxides) for the same samples averaged 1020 ± 460 years.

As noted previously, the fractionation methods applied in this study, based on density and particle size, overlapped in what they measured (Fig. 4). For example, all of the C in Clay$_{XRD}$ is a subset of HF. There is also overlap between the root-free fLF and the C removed when isolating Clay$_{XRD}$. The distribution of isotopes and C among the various fractions for one soil (illustrated as an example in Fig. 4) demonstrate these variations and relationships and show that the biggest differences in radiocarbon are between Clay$_{XRD}$ and root-free fLF fractions.

3.5 Mineral–carbon relationships at the profile scale

Profile-averaged properties were calculated to highlight variation across the landscape (Table 5). This calculation introduced errors associated with highly uncertain estimates of gravel and bulk density (see values in Table S1), but
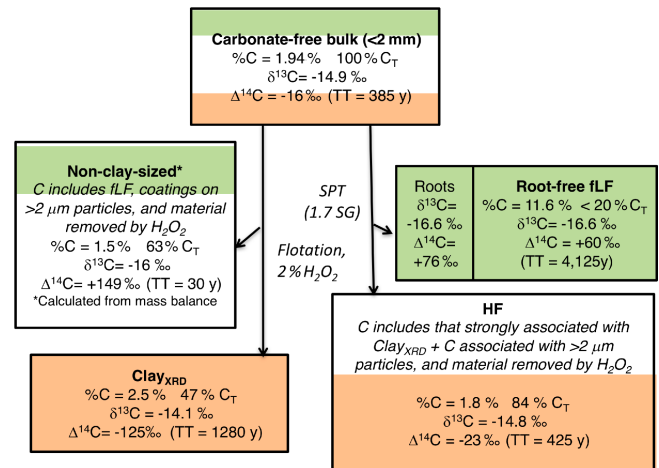

Figure 4. Comparison of C and C isotopes for a single soil sample (0–3 cm depth in GA-740-C (gabbro parent material) indicating the interrelationships among the different process-defined organic C fractions. For each fraction we indicate the percent of total C (C$_T$) it contains; fractions for root-free fLF and HF do not add to 100 % because of contributions from roots picked from the free light fraction (fLF) and C that dissolves in the polytungstate solution and is not recovered. Colors indicate overlaps between C among different fractions that exist. For example, C strongly associated with the clay-sized fraction measured with XRD (Clay$_{XRD}$; orange) makes up part of the HF C. Free low-density C (fLF; green; including both roots picked from the fLF and the root-free fLF fractions) makes up part of the non-clay-sized fraction. Most of the fLF is likely removed from the Clay$_{XRD}$ when it is treated with 2 % H$_2$O$_2$.

as these errors are identical for the elements being compared (e.g., profile-averaged concentrations), the profiles being compared should share systematic biases (i.e., similar operator error). The calculation of total profile C inventories (Table 5) are included to demonstrate the importance of these factors in understanding profile-scale C storage and dynamics. For example, the nephelinite soil had the highest C concentrations (averaging 3.8 %C for the whole profile) but was estimated to have 80–90 % gravel (Table S1), so the estimated C inventory (1.1 kg C m^{-2}) is not the highest when compared to other soils (which ranged from a low of 0.6 kg C m^{-2} in the dry granite soils to 11.4 kg C m^{-2} in the black basalt soils). Thus, it should be remembered that the relationships derived here are for the < 2 mm component of soil.

Mass-weighted mean profile %C$_{\text{organic}}$ correlated significantly with mineral CEC (i.e., CEC corrected for organic matter contribution), and bulk Fe oxyhydroxides determined from Fe(d) to Fe(o) (Fig. 6 and Table S2). Together, bulk Fe oxyhydroxides and nonorganic CEC explained most of the variation in carbon inventory across all soils. We found a significant relationship between the amount of smectite (determined as the % of mass in the clay-sized XRD fraction times the fraction of that mass that was quantified by XRD as smec-

Table 5. Profile-averaged (excluding BC / C horizons) properties for the soils sampled in this study. Averages for C and C isotopes are calculated from bulk values. C inventory (C_{inv}) is the sum for the profile in $kgC\,m^{-2}$. All averages are mass-weighted, except C isotopes which are weighted by the mass of C in each horizon. Smectite content (Smec.) is estimated from multiplying the fraction of total mass in the clay-sized XRD by the %Clay (denoted in the table as Clay and expressed as percent of total mass) by the percent of the clay-sized XRD identified as Smectite (Smec.; Table 2). Profile-averaged values for ditionite citrate extracted iron (Fe(d)) and oxalate extractable iron Fe(o) and aluminum (Al(o)), as well as their difference, a measure of Fe oxyhydroxides in bulk soil, are all expressed as weight % as in mass Fe per 100 g of soil.

Identifier	Depth (cm)	Cinv	pH (wt. %)	CEC*	Clay	Smec.	Fe(d)	Fe(o)	Fe(d)–Fe(o)	Al_o	C_org (gC kg^{-1})	C / N	δ^{13}C (‰)	Δ^{14}C (‰)	TT (year)
RH-450-C	30	1.3	6.8	5.5	1.0	10	2.7	0.1	2.6	0.1	0.066	9.9	−16.2	28.0	230
GR-450-C	23	0.6	6.1	7.7	6.3	46	0.6	0.0	0.6	0.0	0.078	11.9	−20.2	30.4	200
NE-450-C	18	1.1	6.8	61.8	38.7	48	5.4	0.3	4.9	0.2	0.385	11.8	−15.9	9.9	235
BB-450-C	49	11.4	7.7	44.3	42.0	98	1.7	0.2	1.5	0.2	0.156	14.2	−13.5	−140.4	1500
GA-450-C	34	8.6	8.3	25.7	9.9	50	1.9	0.2	1.7	0.2	0.166	na	−15.0	−37.0	550
RB-450-C	70	8.6	7.0	50.1	46.2	93	2.5	0.1	2.4	0.1	0.153	14.8	−12.3	−156.4	1720
GR-550-C	62	3.5	5.4	3.2	14.8	1	0.4	0.1	0.3	na	0.032	21.2	−15.3	12.2	430
GR-550-S	41	1.8	5.1	2.6	7.5	21	0.1	0.0	0.1	na	0.023	19.6	−18.6	51.8	150
GR-550-T	46	3.6	7.0	29.9	42.7	24	0.2	0.1	0.1	na	0.050	14.1	−14.7	24.8	225
MG-550-C	38	2.6	6.9	7.8	15.0	41	1.4	0.3	1.1	0.2	0.082	14.2	−13.8	−68.6	755
GA-740-C1	44	7.0	7.2	37.7	17.7	69	2.6	1.1	1.5	0.4	0.153	12.2	−13.9	−47.5	250
GA-740-C2	25	4.5	7.3	31.5	25.8	25	2.5	2.0	0.5	0.3	0.149	11.9	−13.3	26.9	150
GR-740-C	93	5.1	5.7	7.0	3.7	10	0.4	0.0	0.4	0.0	0.036	14.8	−18.5	88.8	240

Depth indicates the depth to which the in-profile averages were calculated (we excluded BC and C horizons). Values in bold for smectite content (Smec.) were not measured but are assumed based on similar lithology values. We assumed average values for the horizons above and/or below to fill in data for smectite content for depths in a profile where no measurements were available (see Supplement).
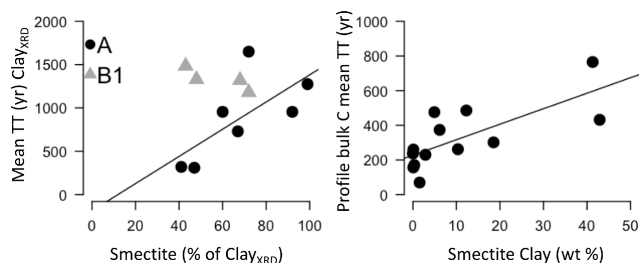

Figure 5. (left) Mean turnover time (TT) of C in the clay-sized XRD fraction increases with smectite concentration; the linear relationship for A horizon points ($n = 7$) is R-squared = 0.48 and $p = 0.08$. (right) Mean TT of bulk C averaged for each profile compared to the fraction of the total C that is found in the clay-sized fraction ($F_{clayXRD}$). The mean TT of bulk organic C correlates significantly with the fraction of organic matter strongly associated with the clay-sized XRD fraction. Here, the linear relationship R-squared = 0.54 and $p = 0.004$.
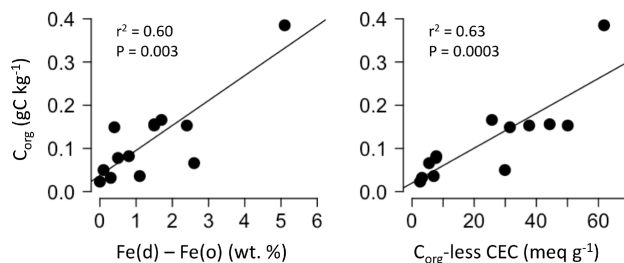
Figure 6. Across all the studied soils, the mean organic C content (gC kg^{-1}) in the soil profile was best predicted by Fe(d)–Fe(o) (left; R-squared = 0.60, $p = 0.003$), and cation exchange capacity corrected for organic matter content (C-corr CEC) (right; R-squared = 0.63, $p = 0.0003$). The best predictors for profile-averaged C turnover times was the amount of smectite clay (Fig. 5 (right)). Correlation matrices for other variables in Table 5 are given as Table S2.

tite minerals) and the mean TT (Fig. 6); total clay-sized XRD fraction and the fraction of smectite each also correlated individually with the horizon averaged bulk ^{14}C, but not as well as their product (see complete correlation matrix in the Supplement, Table S2). The only highly significant correlation for bulk profile ^{13}C was with ^{14}C (Fig. 6), though less significant correlations were found between ^{13}C and average clay content, pH, and CEC (Table S2).

4 Discussion

Geological, climatic, and topographic variation in Kruger National Park give rise to soils of varying mineral compositions. Different strengths of association of organic C with these minerals lead to observed patterns in C inventory and TTs across the sampled landscape. None of the soil properties we measured showed a significant relationship with mean annual precipitation (Table S2), indicating that any influence of climate on C amount and TT was indirect, through mineralogy and possibly vegetation. This was true even for the fractions, like root-free fLF, that are expected to be controlled by vegetation and climate. Underlying lithology sig-

nificantly influenced the amount of clay-sized material, the amount of smectite in this material, CEC, and the TT of bulk C (Table S2).

The variation in mineral composition and amount in Kruger Park allowed us to identify simple, scalable relationships between measures of soil mineralogy with C amount and TT. Overall, we find that no single mechanism can explain both C inventory and TT, partly because our operationally defined fractions failed in most cases (all but the Clay$_{XRD}$ in basalts) to isolate pure mineral end members.

We expected that in soils with low concentrations of SRO minerals, the ratio of smectite to kaoline would exert the strongest influence on C inventory and TT. We indeed observed that the C strongly associated with smectite minerals that made up > 90 % of the clay-sized minerals in basalts had TTs averaging ∼ 1000 years even in the top 2 cm, and overall the TT of C in the Clay$_{XRD}$ fraction correlated (weakly) with the amount of smectite (Fig. 5a).

At the scale of the whole profile, the amount of smectite correlated significantly with mean TT of C (Fig. 5b). Hence, we conclude that the C strongly associated with smectite clay surfaces is responsible for the long TT of C in the clay-sized XRD fraction, and that the total amount of smectite clay in a soil profile exerts control on the overall TTs estimated from ^{14}C of bulk organic C. Soils at the toeslope of the granitic catena with HF C radiocarbon signatures +58 ‰ (i.e., TT of 130 years) still had 39–49 % of their mass in the Clay$_{XRD}$ fraction. In that fraction, ∼ 23–26 % of the mass was identified as smectites and 53–57 % as kaolin clay minerals; Table 2. This example demonstrates that it is not merely the amount of clay-sized material in the soil, but the amount of it that is smectite (i.e., 2 : 1 clay) that is key to long-term C storage in Kruger soils.

These results are in accord with findings by Wattel-Koekkoek and Buurman (2004) that C stabilized on smectite in surface horizons has turnover times of 600–1400 years in soils from Africa and South America. Wattel-Koekkoek et al. (2003) also showed that the older C associated with smectite tends to be more aromatic, suggesting that 2 : 1 clays provide a long-term store for fire-derived C. The aging of LF C with depth in fire-prone soils was shown to be related to the presence of char in soils from other fire-adapted ecosystems (Koarashi et al., 2012; Heckman et al., 2009); where we analyzed this in the red basalt soils, we found increased TT of LF C with depth as well (Table S1). Though we did not measure the chemistry of root-free fLF C, the presence of charred materials provides one possible reason for its low TT, particularly in the red and black basalts where grass biomass is high and fires frequent (Govender et al., 2006).

As is clear from our results, phyllosilicates provide just one mechanism for C storage in ancient soil. Given the very strong relationship between our bulk measure of crystalline Fe oxyhydroxides (i.e., Fe(d)–Fe(o)) and C concentration across our soils (Fig. 6), it is reasonable to propose that Fe oxyhydroxides also provide important mechanisms for stor-

ing organic C, especially in soils with low smectite content. We cannot directly measure the TT of C removed by bulk extractions, as both DCB and oxalate contain dissolved organic C extraneous to the soil. However, we can infer from the relatively short TT of C in soils with fewer smectite minerals that the TT associated with the more abundant mineral phases (kaolinite and Fe oxyhydroxides) is hundreds of years or shorter in A horizons. We thus expect millennial C associated with smectite to remain relatively insensitive to future changes in climate and land use, while the decadal–centennial cycling C associated with the fLF, Fe oxyhydroxides and non-smectite clays like kaolinite should respond faster.

At the pedon scale, clay content was not the best predictor of the amount ($r^2 = 0.50$, $p = 0.02$) or TT ($r^2 = 0.59$, $p = 0.03$) of soil C, though this relationship improved when only smectite clay was considered (Fig. 6; $r^2 = 0.75$, $p = 0.001$). Given the long TT associated with C stabilized by smectite, we conclude that even a small addition of millennially aged C strongly associated with smectite contributes substantially to the mean TT estimated from the bulk soil C. For example, mixing 75 % C with a TT of 25 years with 25 % C with a TT of 1200 years yields a bulk TT of ∼ 320 years. Increasing the millennial pool to 35 % changes the mean TT of bulk C to ∼ 450 years. The same is not true for C stocks, however, which are not significantly correlated with either clay ($r^2 = 0.50$, $p = 0.08$) or smectite clay ($r^2 = 0.45$, $p = 0.12$).

Somewhat unexpectedly, the subhumid-zone gabbro and arid-zone nephelinite soils with the highest concentration of SRO minerals as determined from the Fe(o) and Al(o) extract concentrations had younger C than would be predicted based on expected relationships between SRO minerals and C age found in other soils (see Torn et al., 1997; Kramer et al., 2012). SRO minerals are particularly strong sorbers of C because their hydrated nanocrystals create intimate mixtures of mineral and organic material that – in the absence of drying and rewetting or redox pulses – tend to remain very stable (Chorover et al., 2004; Thompson et al., 2006b; Buettner et al., 2014). However, when SRO minerals are subjected to drying and rewetting or oxidation–reduction pulses, they reorganize into larger, more well-ordered crystalline compounds by ejecting C and water from the interior of their lattice structure (Ziegler et al., 2003; Thompson et al., 2006a). The subhumid-zone gabbro and nephelinite soils had younger C, and only 9–17 % of the C was associated with the clay-sized XRD fraction, even though they have > 5 % SRO mineral concentrations. The young C suggests that the SRO mineral phase is likely a relatively transitory phase that forms as primary minerals in the gravel and cobble fraction of the soil weather and the resulting SRO minerals rapidly ripen to kaolinite, with any C that was sorbed into the SRO mineral phase made available for microbial decomposition. In the same way, redox oscillations under seasonal wet–dry cycles promote crystallinity of Fe and we suggest that the Fe-

bearing SRO minerals in these environments are likely short-lived giving way to crystalline Fe forms where C is sorbed to surfaces rather than within the less accessible lattice (Ziegler et al., 2003; Chorover et al., 2004). Thus, although the availability of a large surface area may promote stabilization of large amounts of C in these soils (e.g., nephelinite in Fig. 3), the relatively rapid TT of that C may be a reflection of the short residence time of the minerals themselves and the short TT of C sorbed onto 1 : 1 clays and crystalline Fe oxyhydroxides. Studies of mineral–carbon interactions must consider not only the strength of C association with various mineral phases (e.g., strong for SRO and smectite, weak for kaolinite and oxyhydroxides), but also the timescale of mineral stability in the soil profile and its pedogenic setting. Where SRO minerals and oxyhydroxides are stable, the associated C tends to be old, but in climates such as in Kruger the combination of a relatively short but strong rainy season and a long intervening dry season can lead to relatively rapid mineral transformation and hence rapid C turnover.

Factors that vary with soil depth exert controls on both C inventory and TT in KNP soils, as has been reported in many other areas. These affect the ^{14}C in all measured fractions. However, the rates at which age increased with depth differed between soils and C fractions. For soils with the largest amount of smectite clays (e.g., basalts), offsets in the TT for clay-sized XRD, and the "non-clay-size" fractions were largest at the surface and smallest at depth. In contrast, in soils with little smectite clay, the offset between fractions was relatively uniform with depth. More work is required to understand the stability of the different mineral phases themselves, especially organic C associated with Fe (and Al) oxyhydroxides phases, and how they interact with transport mechanisms in soil (e.g., Schrumpf et al., 2013; Schrumpf and Kaiser, 2015).

There appears to be a mineral/lithologic control on ^{13}C variation in KNP soils. This control can operate in at least two ways. First, the root-free fLF δ^{13}C seem to indicate greater C3-derived vegetation inputs to soils with more felsic parent materials, and a predominance of C4 inputs in more mafic soils (Fig. 2a). This is consistent with the vegetation patterns on the ground (Scholes et al., 2003), with C4 grasses dominating the basalt-soil landscapes. These patterns are largely preserved in the mineral-associated C (Fig. 2a), although HF δ^{13}C is consistently enriched compared to the LF δ^{13}C. At the profile scale, the strongest predictor of δ^{13}C is Δ^{14}C (or TT; Fig. 6; $r^2 = 0.75$, $p = 0.005$), followed by pH ($r^2 = 0.65$, $p = 0.016$) and clay content ($r^2 = 0.65$, $p = 0.017$). For the isolated clay fraction, the relationship between δ^{13}C and smectite was weak. Soils with the greatest amount of smectite are also those with the greatest C4 vegetation, so it is unclear whether lithologic control on C3 vs. C4 plants or fractionation associated with different mineral stabilization mechanisms is responsible for the overall trends observed in δ^{13}C. Nonetheless, interpretations of paleo-vegetation from bulk soils must be undertaken with

care, as variations in the mechanism of C stabilization across the landscape may affect the δ^{13}C signature as well as vegetation changes. More work is needed to disentangle these relationships at broader spatial scales encompassing climate and topographic gradients that will also involve changes in mineralogy.

Large parts of the land surface contain old soils with low concentrations of SRO minerals (Paton et al., 1995). We found good agreement in the age of C in the most smectite-rich (basalt soils) clay-sized XRD fraction and those reported by Wattel-Koekkoek et al. (2003) from soils collected at other sites in Africa and South America. Smectite clay content may thus provide a useful indicator for the fraction of C stabilized on millennial timescales over large areas. While quantitative clay mineralogy is not an easy measurement, the amount of smectite in our soils was broadly predictable from lithology and from more easily measured soil properties such as CEC (corrected for organic contributions; $r^2 = 0.79$, $p < 0.01$) or pH (when below CaCO$_3$ saturation; $r^2 = 0.83$, $p < 0.005$; Table S2). Thus, across a range of landscapes and parent materials, one could predict how much of the C in soils is cycling on slower timescales based on these parameters, while overall C inventory is more related to crystalline Fe and Al oxyhydroxides.

5 Conclusions

Differences in C cycling among soils differing in lithology, topography and rainfall are largely explained by varying mineralogy. Where SRO mineral concentration is low, the age of C in the clay-sized fraction depends on the concentration of smectite. However, this is only the case in basalts, for soils other than basalts, C TT averaged hundreds of years and is therefore weakly associated with the clay-sized fraction.

Our data indicate that heavy fraction C in old soils consists of two major components: a relatively "passive" pool that stabilizes C for millennia that we suggest is strongly bound to smectite, and a more dynamic pool stabilized for decadal to centennial timescales that includes C bound to kaolinite and/or associated with crystalline Fe and Al (oxy)hydroxides. Most C in surface horizons, even in basalt soils where clays are > 95 % smectite, is in this faster-cycling pool. A small but highly dynamic light fraction pool that is more reflective of vegetation also occurs in all soils. Increases in age of C with depth in soil profiles may indicate rates of vertical mixing or the time required for repeated sorption/release of C as it moves downwards, or it may reflect changes in the stability of the minerals themselves as a function of soil depth. While more research will be needed to understand these issues, our results hold great promise for predicting C inventory and TT based on intrinsic timescales of C stabilization mechanisms.

Information about the Supplement

Data are provided in the Supplement as an Excel spreadsheet; metadata for the spreadsheet are given in the supplemental text.

The Supplement related to this article is available online at doi:10.5194/soil-3-17-2017-supplement.

References

Bern, C. R., Chadwick, O. A., Hartshorn, A. S., Khomo, L. M., and Chorover J.: A mass-balance model to separate and quantify colloidal and solute redistributions in soil, Chem. Geol., 282, 113–119, 2011.

Buettner, S. W., Kramer, M. G., Chadwick, O. A., and Thompson, A.: Mobilization of colloidal carbon during iron reduction in basaltic soils, Geoderma, 221–222, 139–145, 2014.

Castanha, C., Trumbore, S., and Amundson, R. G.: Methods of separating soil carbon pools affect the chemistry and turnover time of isolated fractions, Radiocarbon 50, 83–97, 2008.

Chadwick, O. A., Roering, J. J., Heimsath, A. M., Levick, S. R., Asner, G. P., and Khomo, L. M.: Shaping post-orogenic landscapes by climate and chemical weathering, Geology, 41, 1171–1174, 2013.

Chorover, J., Amistadi, M. K., and Chadwick, O. A.: Surface charge evolution of mineral-organic complexes during pedogenesis in Hawaiian basalt, Geochim. Cosmochim. Ac., 68, 459–476, 2004.

Eberl, D. D.: User's guide to RockJock, a program for determining quantitative mineralogy from powder X-ray diffraction data, US Geological Survey Open-File Report 2003-78, 47 pp., 2003.

Gaudinski, J. B., Trumbore, S. E., Davidson, E. A., and Zheng, S.: Soil carbon cycling in a temperate forest: radiocarbon-based estimates of residence times, sequestration rates, and partitioning of fluxes, Biogeochemistry 51, 33–69, 2000.

Govender, N., Trollope, W. S., and Van Wilgen, B. W.: The effect of fire season, fire frequency, rainfall and management on fire intensity in savanna vegetation in South Africa, J. Appl. Ecol., 43, 748–758, 2006.

Harrell Jr., F. E. with contributions from Charles Dupont and many others: Hmisc: Harrell Miscellaneous, R package version 3.17-2, https://CRAN.R-project.org/package=Hmisc (last access: 10 October 2016), 2016.

Heckman, K., Welty-Bernard, A., Rasmussen, C., and Schwartz, E.: Geologic controls of soil carbon cycling and microbial dynamics in temperate conifer forests, Chem. Geol., 267, 12–23, 2009.

Khomo, L., Hartshorn, A. S., Rogers, K. H., and Chadwick, O. A.: Impact of rainfall and topography on the distribution of clays and major cations in granitic catenas of southern Africa, Catena, 87, 119–128, 2011.

Khomo, L., Bern, C. R., Hartshorn, A. S., Rogers, K. H., and Chadwick, O. A.: Chemical transfers along slowly eroding catenas developed on granitic cratons in southern Africa, Geoderma, 202–203, 192–203, 2012.

Koarashi, J., Hockaday, W. C., Masiello, C. A., and Trumbore, S. E.: Dynamics of decadally cycling carbon in subsurface soils, J. Geophys. Res.-Biogeo., 117, 2156–2202, 2012.

Kramer, M. G., Sanderman, J., Chadwick, O. A., Chorover, J., and Vitousek, P. M.: Long-term carbon storage through retention of dissolved aromatic acids by reactive particles in soil, Glob. Change Biol., 18, 2594–2605, doi:10.1111/j.1365-2486.2012.02681.x, 2012.

Lawrence, C. R., Harden, J. W., Xu, X., Schulz, M. S., and Trumbore, S. E.: Long-term controls on soil organic carbon with depth and time: a case study from the Cowlitz River Chronosequence, WA USA, Geoderma, 247–248, 73–87, 2015.

Masiello, C. A., Chadwick, O. A., Southon, J., Torn, M. S., and Harden, J. W.: Weathering controls on mechanisms of carbon storage in grassland soils, Global Biogeochem. Cy., 18, GB4023, doi:10.1029/2004GB002219, 2004.

Mehra, O. and Jackson, M.:, Iron oxide removal from soils and clays by a dithionite-citrate system buffered with sodium bicarbonate, Proc. 7th Nat. Conf. Clays., 1960.

Paton, T. R., Humphreys, G. S., and Mitchell. P. B.: Soils: A New Global View, Routledge, Taylor and Francis, New York, 1995.

Poch, O., Jaber, M., Stalport, F., Nowak, S., Georgelin, T., Lambert, J. F., Szopa, C., and Coll, P.: Effect of nontronite smectitie clay on the chemical evolution of several organic molecules under simulated Martian surface ultraviolet radiation conditions, Astrobiology 15, 1–17, 2015.

Pollastro, R. M.: A recommended procedure for the preparation of oriented clay-mineral specimens for x-ray diffraction analysis: Modifications to Drever's filter membrane peel technique, USGS Open-File Report 82–71, 24 pp., 1982.

R Core Team.: CorreR: A language and environment for statistical computing. R Foundation for Statistical Computing, Vi-

enna, Austria, https://www.R-project.org/ (last access: 15 October 2016), 2015.

Scholes, R. J., Bond, W. J., and Eckhardt, H. C.: Vegetation dynamics in the Kruger ecosystem, in: Ecology and Management of Savanna Heterogeneity, edited by: du Toit, J. T., Rogers, K. H., and Biggs, H. C., Island press, Corvelo, 2003.

Schrumpf, M. and Kaiser, K.: Large differences in estimates of soil organic carbon turnover in density fractions by using single and repeated radiocarbon inventories, Geoderma, 239, 168–178, 2015.

Schrumpf, M., Kaiser, K., Guggenberger, G., Persson, T., Kögel-Knabner, I., and Schulze, E.-D.: Storage and stability of organic carbon in soils as related to depth, occlusion within aggregates, and attachment to minerals, Biogeosciences, 10, 1675–1691, doi:10.5194/bg-10-1675-2013, 2013.

Schwertmann, U.: Use of oxalate for Fe extraction from soils, Can. J. Soil Sci., 53, 244–246, 1973.

Sierra, C. A., Müller, M., and Trumbore, S. E.: Modeling radiocarbon dynamics in soils: SoilR version 1.1, Geosci. Model Dev., 7, 1919–1931, doi:10.5194/gmd-7-1919-2014, 2014.

Soil Survey Staff.: Kellogg Soil Survey Laboratory Methods Manual. Soil Survey Investigation report No. 42, Version 5.0., edited by: Burt, R. and Soil Survey Staff, US Department of Agriculture, Natural Resources Conservation Service, 2014.

Sollins, P., Kramer, M. G., Swanston, C., Lajtha, K., Filley, T., Aufdenkampe, A. K., Wagai, R., and Bowden, R. D.: Sequential density fractionation across soils of contrasting mineralogy: evidence for both microbial-and mineral-controlled soil organic matter stabilization, Biogeochemistry, 96, 209–231, 2009.

Steinbeiss, S., Temperton, V., and Gleixner, G.: Mechanisms of short-term soil carbon storage in experimental grasslands, Soil Biol. Biochem., 40, 2634–2642, 2008.

Stuiver, M. and Polach, H.: Reporting of ^{14}C data, Radiocarbon, 19, 355–363, 1977.

Thompson, A., Chadwick, O. A., Rancourt, D. G., and Chorover, J.: Iron-oxide crystallinity increases during soil redox oscillations, Geochim. Cosmochim. Ac., 70, 1710–1727, 2006a.

Thompson, A., Chadwick, O. A., Boman, S., and Chorover, J.: Colloid mobilization during soil iron redox oscillations, Environ. Sci. Technol., 40, 5743–5749, 2006b.

Torn, M. S., Trumbore, S. E., Chadwick, O. A., Vitousek, P. M., and Hendricks, D. M.: Mineral control of soil organic carbon storage and turnover, Nature, 389, 170–173, 1997.

Trumbore, S.: Radiocarbon and soil carbon dynamics, Annual Rev. Earth Pl. Sc., 37, 47–66, 2009.

Venter, F. J., Scholes, R. J., and Eckhardt, H. C.: The abiotic template and its associated vegetation pattern, in: The Kruger Experience: Ecology and Management of Savanna Heterogeneity, edited by: du Toit, J. T., Rogers, K. H., and Biggs, H., Island Press, Washington, DC, 83–129, 2003.

Wattel-Koekkoek, E. J. W. and Buurman, P.: Mean residence time of kaolinite and smectite-bound organic matter in Mozambiquen soils, Soil Sci. Soc. Am. J., 68, 154–161, 2004.

Wattel-Koekkoek, E. J. W., Buurman, P., Van Der Plicht, J., Wattel, E., and Van Breemen, N.: Mean residence time of soil organic matter associated with kaolinite and smectite, Eur. J. Soil Sci., 54, 269–278, 2003.

Xu, X., Trumbore, S. E., Zheng, S., Southon, J. R., McDuffee, K, Luttgen, M., and Liu,, J. C.: Modifying A Sealed Tube Zinc Reduction Method for Preparation of AMS Graphite Targets: Reducing Background and Attaining High Precision, Nucl. Instrum. Meth. B, 259, 320–329, doi:10.1016/j.nimb.2007.01.175, 2007.

Ziegler, K., Hsieh, J. C. C., Chadwick, O. A., Kelly, E. F., Hendricks, D. M., and Savin, S. M.: Halloysite as a kinetically controlled end product of arid-zone basalt weathering, Chem. Geol., 202, 461–478. 2003.